Spectrochimica Acta Part B 131 (2017) 58–65

Contents lists available at ScienceDirect

Spectrochimica Acta Part B

journal homepage: www.elsevier.com/locate/sab

Quantitative analysis of metals in waste foundry sands by calibration free-laser induced breakdown spectroscopy

D.M. Díaz Pace [a,*], R.E. Miguel [b], H.O. Di Rocco [a], F. Anabitarte García [c], L. Pardini [d], S. Legnaioli [d], G. Lorenzetti [d], V. Palleschi [d]

[a] Centro de Investigaciones en Física e Ingeniería del Centro de la Provincia de Buenos Aires (CIFICEN), CONICET, CICPBA, Fac. Cs. Exactas UNCPBA, Campus Universitario, (B7000GHG) Tandil, Buenos Aires, Argentina
[b] National Institute of Agricultural Technology, EEA INTA Chilecito, Ruta de la Producción Km 7,5 (5360) Tilimuqui, Chilecito, La Rioja, Argentina
[c] Photonic Engineering Group, Universidad de Cantabria, Edificio I+D+iTelecomunicación, Dpto. TEISA, 39005 Santander, Spain
[d] Institute of Chemistry of Organometallic Compounds, Research Area of National Research Council, Via G. Moruzzi, 1, 56124 Pisa, Italy.

ARTICLE INFO

Article history:
Received 22 August 2016
Received in revised form 3 March 2017
Accepted 9 March 2017
Available online 10 March 2017

Keywords:
Laser-induced breakdown spectroscopy
LIBS
Waste sand
Plasma characterization

ABSTRACT

Laser-induced breakdown spectroscopy (LIBS) was applied for quantitative analysis of the elemental composition of waste molding and core sands produced from industry as part of the casting process. To perform the analysis, waste foundry sands (WFS) were collected from metalcasting foundries and prepared in the form of solid pellets with the addition of polyvinyl alcohol as binder. The measurements were carried out using the Mobile double pulse instrument for LIBS analysis (Modì). The spectral analysis was carried out with the calibration-free approach (CF-LIBS). Metal elements commonly found in WFS including Al, Ba, Fe, Li, Mg, Mn, Pb, Ti, Zr, and Zn, were detected and quantified. The metal concentrations for WFS were compared with virgin sand to assess the influence of the casting material as well as the binders used in the foundries to reclaim the sands. The results demonstrated the feasibility of LIBS method as an alternative or complementary technique for the chemical characterization of WFS.

1. Introduction

Approximately 100 million tons of waste foundry sand (WFS) is annually generated worldwide by foundry industry to create molds and cores for metalcasting [1]. The molding sands are manufactured by using virgin sands with the addition of binding agents (e.g.: bentonite clay, organic resins). At the end of the casting process, the molds or cores are broken apart to retrieve the pieces and to be further reclaimed. However, after some time of reuse sand is discarded and replaced with new sand. The WFS originated are typically sent to landfills. Thus, research have been carried out on the beneficial use of WFS in geotechnical (e.g.: concrete, asphalt, and road-subbase) and agricultural applications (e.g.: manufactured soils) [2–4]. On the other hand, other studies have examined the possible metal leaching of WFS ([5] and references therein). For the different metal cast and binder types analyzed, it was concluded that in general the metal concentrations are similar to those present in common sand. Nevertheless, in some cases the concentration of heavy metals were found elevated respect to virgin sand, which raises a concern of prime importance for human health and environmental pollution. In this context, assessing an analytical tool for rapid monitoring of hazardous metals in WFS would be of great interest in many different areas of industry as well as in environmental studies since usual laboratory methods; e.g.: X-ray diffraction, do not match these requirements because of performance limitations [6].

Laser-Induced Breakdown Spectroscopy (LIBS) is a versatile technology for quantitative elemental analysis of various contaminants in a wide range of samples including soils, sediments, and other geological materials [7]. LIBS technique is based on spectral analysis of the radiation emitted by a laser-induced plasma (LIP) generated with the material ablated from the target for the determination of the chemical composition of gases, liquids, and solids [8–10]. The physics of LIP generation and its temporal evolution are described in detail elsewhere [11]. In contrast to many other common techniques requiring complex and time consuming procedures, the inherent features of simplicity and versatility make LIBS the technique of choice to carry out rapid, on site, multi-element measurement with a minimum of sample preparation. Furthermore, a small amount of sample is required for the analysis, is able to detect light elements such as H, Li, B, C, N, and O, which are not detected by other analytical methods, and can used in a

* Corresponding author at: Pinto 399, (B7000GHG) Tandil, Buenos Aires, Argentina.
E-mail address: ddiaz@exa.unicen.edu.ar (D.M. Díaz Pace).

http://dx.doi.org/10.1016/j.sab.2017.03.007
0584-8547/

hyphenated approach with another techniques such as Raman and laser-induced fluorescence. Typical detection limits for LIBS are in the ppm range.

The use of LIBS for material analysis is based on the fact that characteristic peaks in the spectrum emitted by the LIP in the UV–Vis spectral range (200–900 nm) contain the unique spectral signature of all the elements of the periodic table; thus, the elements present in the sample are identified by their "chemical fingerprints". Elemental concentrations are related to the corresponding emission intensities, assuming that the plasma composition is representative of that of the sample previous to the laser ablation (stoichiometric ablation). Nevertheless, performing quantitative analysis is not straightforward because the emission intensity of a given specie in the LIP is strongly affected by the experimental conditions under which it was generated; namely, laser parameters, sample features, and surrounding atmosphere [12]. Moreover, in applications carried out in air at atmospheric pressure the main difficulties for spectroscopic analysis come from transient plasma evolution, spatial inhomogeneity, self-absorption, and matrix effects [13,14]. These issues affect the quality, accuracy and precision of the results. Therefore, laboratory tests are of major importance for evaluating and optimizing the analytical performance of LIBS aimed at achieving reliable quantitative results.

From an experimental point of view, the most common approach to perform quantitative LIBS analysis relies on the construction of calibration curves employing matrix-matched standards. However, in many practical situations reference samples are often either limited or unavailable, as it is often the case with geological and environmental samples. Calibration-free LIBS (CF-LIBS) is an alternative method based on plasma characterization for performing quantitative analysis without the need for calibration samples [15]. Satisfactory results have been obtained with CF-LIBS in a wide range of solid materials including geological samples such as minerals and rocks.

The recent reviews by Harmon et al. [16] and Senesi [17] summarize the current state-of-the-art on applications of LIBS for the analysis of geological and environmental samples. However, only a few studies have been reported in the pertinent literature dealing with quantitative analysis of elements in sand samples. Krasniker et al. [18] investigated matrix effects in sand–soil mixtures by measuring the emission intensities of trace elements. Harris et al. [19] reported the determination of the content of N in soil samples using sand as a surrogate. Haider et al. [20] used LIBS technique for the identification of valuable minerals in beach sands. The content of Ti was quantified by constructing a calibration curve with reference samples specifically manufactured with sand. In a second work, the analysis was extended for the simultaneous detection of rare earth elements, and others, in raw monzanite sands [21].

The aim of the present work was to evaluate the potential of the CF-LIBS method for multi-elemental quantitative analysis of WFS. For this purpose, a set of WFS samples of different nature were analyzed for total content of metal elements. The information of this study will be useful to potential environmental and industrial applications.

2. CF-LIBS method for quantitative analysis

CF-LIBS is a method capable of providing analytical quantitative results without employing calibration standards, thus also avoiding matrix effects. It is based on LIP characterization in the acquisition time window through the determination of the temperature, electron density and atom/ion densities of the detected elements. We refer the reader to Ref. [15,22] for a detailed description of its main characteristics and the underlying hypothesis.

The CF-LIBS approach relies on modeling the LIP as an ideal plasma. Thus, the following conditions are assumed: stoichiometric laser ablation, local thermodynamic equilibrium (LTE), spatial and temporal homogeneity, and optical thinness of the spectral lines included in the calculations. In LTE condition, the standard statistic distributions are used, i.e.: the excited levels are populated according to the Boltzmann distribution and ionization states are populated according to the Saha–Boltzmann equilibrium equations [23]. Under the above mentioned assumptions, the measured integrated spectral line intensity I_{ji} ($J\,s^{-1}\,m^{-1}\,sr^{-1}\,nm^{-1}$) emitted along the line of sight is given by solution to the equation of radiation transfer [24,25],

$$I_{ji} = F\frac{hc}{4\pi\lambda_0} n_s A_{ji} \frac{g_j}{U_s(T)} e^{-E_j/kT} \quad (1)$$

where λ_0 (m) is the central wavelength of transition, n_s (m^{-3}) is the number density of the emitting species s in the plasma, A_{ji} (s^{-1}) is the transition probability, g_j (dimensionless) and E_j (eV) are the degeneracy and the energy of the upper energy level respectively, U_s (T) (dimensionless) is the partition function of the species s, kT (eV) is the plasma temperature, and F is and unknown experimental factor depending on the instrumental set-up and accounting for the absolute efficiency and units.

In LIBS experiences, Stark broadening is the predominant mechanism that determines the Lorentzian contribution to line profiles in comparison with the Doppler broadening and the other pressure broadening mechanisms [23]. As broadening effects are strongest for atoms showing linear Stark effect, the H lines present the largest broadenings. In fact, typical Stark width of H lines is by an order of magnitude larger than that of heavier elements. When LIBS measurements are carried out in air, the H_α emission is generally originated from the very small concentration of natural humidity in the ambient. Thus, the electron density n_e (cm^{-3}) is independently calculated by using the experimentally measured Stark width of the Balmer line H_α at 656.28 nm [26]. Namely,

$$n_e = 8.02\,x\,10^{12}\left(\frac{\Delta\lambda_{1/2}}{\alpha_{1/2}}\right)^{3/2} cm^{-3} \quad (2)$$

where $\Delta\lambda_{1/2}$ is the Lorentzian line width (FWHM) of the H_α line, and $\alpha_{1/2}$ is the half width (HWFM) of the reduced Stark profiles, which is a weak function of the electron density and temperature. The values of $\alpha_{1/2}$ are tabulated in Table III.a of Ref. [27].

3. Experimental

3.1. Samples

The samples used for this study were WFS collected from foundries located in the province of Buenos Aires (Argentina). The selected analytical set was composed of seven samples (S1–S7) manufactured using silica sand and different unknown binding agents. One additional sample of virgin silica sand (S0) was also obtained from the foundries feedstock without further treatment other than drying for comparative purposes.

Sand is a naturally occurring granular material composed of rock and mineral particles with a widespread composition and grain size. Hence, the samples were firstly crushed in a ball mill for 2 min to reduce the particle size and then prepared in the form of pellets with a binder to improve cohesion. For each sample, 4 g of sand were mixed with 0.5 g of polyvinyl alcohol (PVA; Merck, molecular formula $(C_2H_4O)_x$) in powder form diluted with 5 ml of hot distilled water. The mixture was well stirred to homogenize it, poured in a plastic die, and left dry at room temperature until it was harden. In this way, pellets of approximately 3 cm of diameter, 0.5 cm of thickness, and 4.5 g of weight were manufactured for subsequent LIBS analysis (Fig. 1).

3.2. Experimental setup

The sand samples were analyzed using the Modì "Smart" instrument developed by the Applied Laser Spectroscopy Laboratory at CNR (Pisa, Italy) in collaboration with Marwan Technology s.r.l. [28,29]. Modì is a transportable LIBS instrument which has been widely tested for

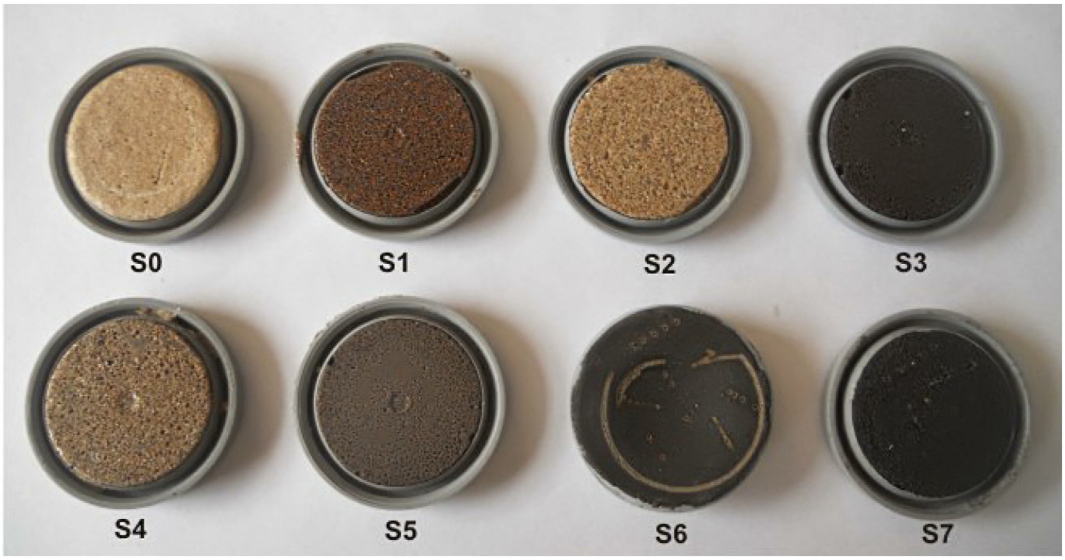

Fig. 1. Sand samples analyzed in this work (diameter = 3 cm).

chemical analysis of art and archeological objects [30–34]. The experimental arrangement is sketched in Fig. 2. Two collinear laser pulses at Nd:YAG fundamental wavelength (1064 nm) are delivered on the target with an energy up to 80 mJ per pulse with a FWHM of about 10 ns at a maximum repetition rate of 10 Hz. In our experiment, the pulse energy was 50 mJ per pulse and the interpulse delay was set at 1 μs. The laser beam is focused on the target by a f = 10 cm converging lens; the plasma emission was collected by an optical fiber placed at 10 mm distance from the laser spot on the target, at a 45 degrees angle. In this arrangement the emission of the whole plasma was collected for the spectral analysis and transferred to a dual-channel broadband Avantes mini-spectrometer equipped with a CCD detector and covering the spectral range between 200 and 900 nm with a resolution of 0.1 nm in the range 200–430 nm and 0.3 nm from 430 to 900 nm. The response curve of the optical system was measured using a certified Deuterium–Halogen lamp (Avalight from Avantes). The LIBS spectrum acquisition was triggered 2 μs after the second laser pulse to avoid the initial continuum emission and the acquisition time was 2 ms, which was typically much longer than the plasma lifetime. Although the spectral acquisition was non time-resolved, in a recent paper Grifoni et al. demonstrated the possibility of using this kind of spectrometer for the measurement of the main plasma parameters used for CF-LIBS analysis (electron temperature and number density) with an equivalent time integration window of about 1 microsecond [35]. The measurements were taken in 5 different points of the samples, averaging 10 consecutive laser (double) pulses after 10 cleaning shots. The 5 resulting LIBS spectra were further averaged to obtain a single spectrum representative of each sample. In such experimental conditions, spectra with an appropriate signal-to-noise ratio (SNR) were recorded.

4. Results and discussion

4.1. Analytical lines and measurements

Broadband LIBS spectra were measured from all sand samples. A typical spectrum is shown in Fig. 3, where a few emission lines for detected elements are highlighted. The identified elements included Si, Fe, C, Mn, Mg, Ti, Al, Ca, Sr, Ba, Na, Li, K, H, O, N, Zr, and Pb whose characteristic spectral lines were measured from all the samples with different intensities.

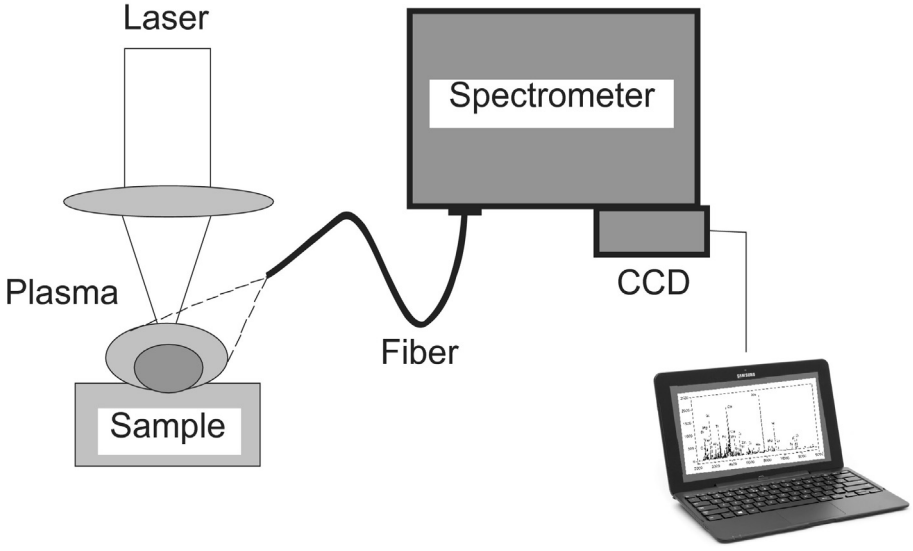

Fig. 2. Experimental LIBS arrangement.

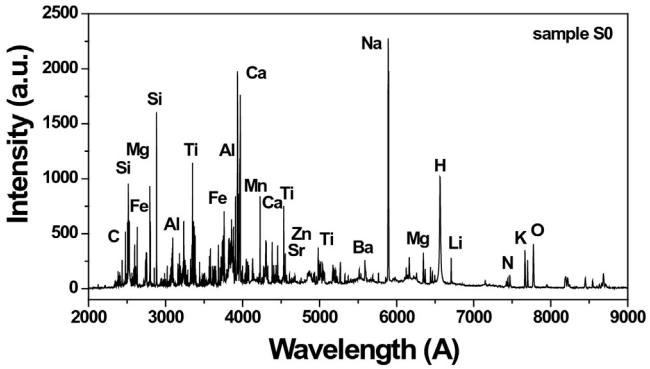

Fig. 3. Broadband LIBS spectrum from virgin sand sample (S0).

The spectral lines measured for each element (Table 1) corresponded to transitions belonging to neutral atomic and singly ionized species with available atomic data from NIST database [36]. The number of analytical lines was different for each element, it varied from one line (H, Pb, Zn) to a hundred lines (Fe). The chemical composition of the different sands was quantitatively determined via the CF-LIBS method described in Section 2, based on characterizing the LIP with the measured line intensities. To perform the analysis, the measurement of spectral lines of all the elements present in the samples is required. Despite undetected traces with concentrations lower than detection limits of the instrument may be present, they do not affect significantly the overall concentration through the closure condition and can be neglected [15].

Table 1
Main analytical spectral lines of neutral (I) and single ionized (II) elements employed for CF-LIBS analysis of sand samples.

Species	# Lines	Main emission lines (Å)
Al I	4	3082.1, 3092.8, 3944.0, 3961.5
Al II	1	3586.0
Ba I	1	5535.5
Ba II	3	4934.1, 6141.7, 4554.0
C I	1	2478.6
Ca I	25	4226.7, 4307.7, 4318.6, 4454.8, 5265.6, 5594.6, 6162.2
Ca II	8	3158.9, 3179.3, 3706.4, 3736.9, 3933.7, 3968.5, 8542.1, 8662.1
Fe I[a]	78	2490.6, 3020.6, 3067.2, 3570.1, 3687.4, 3745.6, 3749.5, 3763.8, 3856.4, 3859.9, 4325.8, 4383.5 4404.7
Fe II[a]	34	2354.5, 2404.9, 2585.9, 2599.4, 2611.9, 2739.5, 2746.5, 2749.3
H[b]	1	6563.0
K I	3	5339.7, 7664.9, 7699.0
Li I	1	6707.8
Mg I	6	2779.9, 2783.0, 2852.1, 3838.3, 5167.3, 5183.6
Mg II	4	2795.5, 2798.0, 2802.7, 6346.7
Mn I	2	4030.8, 4033.1
Mn II	1	2576.1
N I	7	7423.6, 7442.3, 7468.3, 8184.9, 8188.0, 8242.4, 8685.3
Na I	3	5889.9, 5895.9, 8194.8
O I	3	7774.2, 7949.0, 8446.4
Si I	14	2881.6, 2434.9, 2506.9, 2516.1, 2519.2, 2524.2, 2528.5, 2631.3, 6125.0
Si II	2	4130.9, 6371.4
Sr I	3	4607.3, 4868.7, 4892.0
Sr II	2	4215.5, 4077.7
Ti I	27	3341.9, 3642.7, 3653.5, 3904.8, 3981.8, 3998.6, 4534.8, 4548.8, 4981.7, 4991.1, 4999.5, 5007.2, 5014.2, 5038.4
Ti II	34	3239.0, 3349.4, 3361.2, 3372.8, 3383.8, 3759.3, 3761.3
Pb I[c]	1	4057.8
Zn I	1	3302.6
Zr I[d]	8	3601.2, 4582.3, 4687.8, 4710.1; 4739.5, 4772.3, 4815.0; 4824.3
Zr II[d]	6	3392.0, 3438.2, 3496.2, 3576.8, 3674.1, 3698.2

[a] Employed for calculation of plasma temperature.
[b] Employed for calculation of plasma electron density.
[c] Detected in sample S4.
[d] Detected in samples S5 and S6.

In LIBS applications carried out at in air atmosphere the achievement of an accurate plasma characterization is usually hindered by self-absorption of spectral lines and spatial inhomogeneity of the plume. Several methods have been proposed to compensate self-absorption [37–43]. An automated recursive algorithm (SAC: Self-Absorption Correction) based on the curve of growth can be applied in CF-LIBS method for correcting the line intensities of self-absorbed lines [37]. Further, models of inhomogeneous plasmas have been reported [44–49], but these are intrinsically more elaborated and time-consuming, which may reduce their practical applicability. Line overlapping and spectral interference are additional concerns for the analysis of complex multi-element samples, such as sand. Furthermore, recording many emission lines is advisable to carry out both, Boltzmann and Saha–Boltzmann plots.

Therefore, all the analytical lines were included in the CF-LIBS routine despite not being optimum for quantitative analysis, SAC procedure was not used, and a homogeneous plasma was assumed. One exception was the H_α line for which self-absorption was evaluated, as described in the following section.

4.2. Plasma characterization

The plasma electron density was calculated through the Stark width (w_{Stark}) of the H_α line ($\lambda = 6563$ Å) according to Eq. (2). The H_α lines recorded from the samples were isolated and with a good SNR allowing an accurate determination of the electron density. In our experiment, the H emission is due to ambient air and PVA. Hence, a possible self-absorption of the H_α line was evaluated. In fact, self-absorption will have the effect of broadening the H_α line producing an apparently larger Stark width and, then, an over-estimation of the electron density. An inaccurate value of the electron density will cause a vertical shift of the coordinates of ionic lines on the Saha–Boltzmann plot which will affect the slope obtained from the linear regression and, finally, the plasma temperature.

Due to the large Stark broadening of the H_α line, the spectral resolution of our experimental setup allowed a detailed measurement of the line profile. Therefore, the analysis of the experimental spectral lines of H_α lines was carried out employing a method similar to that reported in previous works, based in modeling emission line profiles for an arbitrary optical thickness under the framework of a homogeneous plasma in LTE [50]. The method does not require a previous estimation of plasma parameters or construction of curves of growth, so the experimental lines were rapidly analyzed by a computer algorithm developed in MatLab® environment. The emission lines were calculated and matched to the experimental ones through a least-squares iterative fitting procedure based on the calculus of the optical thickness.

The observed mean FWHM of the H_α lines was $w_{FWHM} = (15 \pm 1)$ Å. In the calculus procedure, each experimental H_α line was fitted to an intrinsic line profile dominated by Stark broadening with and a wavelength-dependent optical thicknesses $\tau_\lambda = L(\tau_0, w_{Stark})$. The line profile was represented by a normalized Lorentz function depending on two fitting parameters: its maximum at the line center (τ_0), and the Stark width (w_{Stark}). The Doppler width, estimated from the plasma temperature, was $w_D \approx 0.50$ Å and can be neglected respect to w_{Stark}. The intrinsic line profile was convoluted with the instrument profile, represented by a Gaussian profile with a fixed width $w_G \approx 1.40$ Å. The fitting routine was run until the deviation of the theoretical from the experimental line was minimized and, hence, the profiles that best reproduced the measured lines were obtained along with its optical thicknesses. Next, the self-absorption coefficient; i.e.: $SA \equiv 1 - (1 - e^{-\tau 0}) / \tau_0$, was calculated. It should be noted that SA was defined here slightly different than that in Ref. [38,41], in such a way that $SA = 0$ (or 0% absorbed) if the line is optically thin and it increases up to 1 (or 100%) as the line becomes self-absorbed. The effect of self-absorption

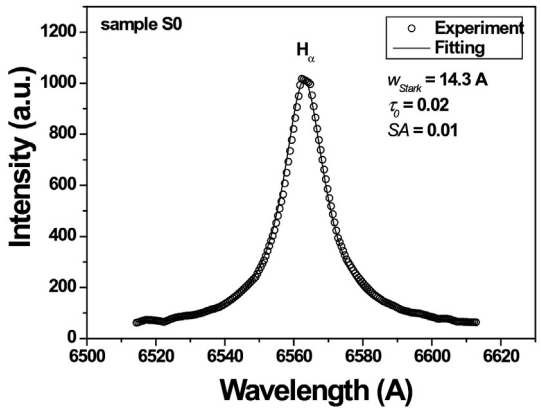

Fig. 4. Example of analysis of the experimental profiles for the H_α lines. The obtained values for Stark width w_{Stark}, maximum optical thicknesses τ_0, and self-absorption coefficient *SA* are shown.

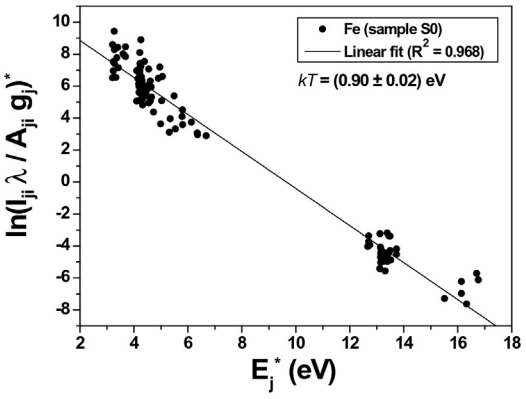

Fig. 5. Saha–Boltzmann plot constructed with Fe I–II lines. Linear fitting and apparent temperature are shown.

starts to be appreciable when $\tau_0 \approx 1$, and thus $SA \geq 0.35$. In our experimental conditions, the *SA* coefficients were ≤0.015 for the H_α lines recorded from all the samples (Fig. 4). Therefore, the total H concentration in the plasma was sufficiently low to consider self-absorption of the H_α line negligible. The Stark widths obtained were in the range 13–15 Å, in agreement with the values reported in other works [26,51].

In addition, for a normalized Lorentzian function the product of its maximum height (L_0) and FWHM (w_L) is constant, namely $L_0.w_L = 2 / \pi \approx 0.64$ [52]. This can be used as a rule of thumb to check if a line was emitted under optically thin conditions by evaluating it for its intrinsic line shape. In our case, $L_0.w_L$ was found on the average to be 0.63 ± 0.01 for the intensity peaks and Stark widths retrieved from the analysis of the H_α lines. Thus, the optically thin emission of the H_α lines in our experiment was further verified.

The average electron density, calculated by using Eq. (2), was $N_e = (1.9 \pm 0.1) \times 10^{17}$ cm^{-3}. The errors corresponded to the standard deviation of the values obtained from the different samples. The N_e values obtained from the different samples were close within the uncertainty of measurement. A criterion proposed by McWhirter [53] necessary to satisfy LTE conditions in a plasma is based on the existence of a critical electron density N_e^0 for which the collisions with electrons dominate over the radiative processes, namely, $N_e^0 = 1.6 \times 10^{12} T^{1/2} (\Delta E)^3$ cm^{-3}, where T (K) is the temperature and ΔE is the energy gap difference between the transition levels. The critical electron number density value was $N_e^0 \sim 1 \times 10^{15}$ cm^{-3}; however, no additional measurements [13] were performed and therefore LTE condition was assumed.

The accuracy of temperature determination depends on the availability of atomic and ionic spectral lines with large difference in the excitation energies of upper levels. Thus, the plasma temperature was obtained from a Saha–Boltzmann plot of Fe I–II lines. Fe was selected because it is the element with the largest number of transitions with known atomic data in the UV–Vis spectral range. In the Saha–Boltzmann plots obtained from the different samples, the data points were low scattered ($R^2 \geq 0.960$) and the majority of Fe lines followed a linear trend (Fig. 5). The average temperature was $kT_{Fe} = (0.90 \pm 0.02)$ eV. The error corresponded to the standard deviation of the values. The kT values obtained from the different samples were close within the uncertainty of measurement.

It should be stressed that the results presented; i.e.: temperature, electron and atom/ion densities, have been derived from spectra obtained via time- and spatial-integration of the measured emission intensities. Hence, as described in [54], the plasma parameters corresponded to apparent values as a result of population-averaged values over the real spatial–temporal distribution of species emissivity along the line of observation.

4.3. Quantitative analysis of WFS

In order to obtain quantitative results for major, minor, and trace components of the sand samples, the CF-LIBS concentrations of the different species detected were calculated by the intercepts q_s derived from the linear regressions of the corresponding Boltzmann plots carried out with a fixed slope; i.e.: $m = -1 / kT_{Fe}$.

A typical output of the CF-LIBS procedure is shown in Fig. 6 for the overall elemental composition of sample S0, evidencing the wide range of compositions measured for sand samples. Major elements with concentrations at percent levels indicated a sand matrix mainly composed by silicates and Al-rich clays. In addition, N, O, and C were detected. Minor elements with concentrations ranging from 0.1 to 0.25 wt% suggested the presence of Fe and Ti compounds, as well as H. Several trace components were determined with concentrations from a few to 500 ppm. Concentrations of N, O, C, and H were included in Fig. 6 for consistency. Actually, contributions due to both, the surrounding ambient air excited by the plasma plume and the binder, respect to the sample composition is presumed. To estimate the concentrations of these elements in the samples, LIBS analysis should be carried out at a reduced air pressure or under a noble gas atmosphere (e.g.: Ar, Ne).

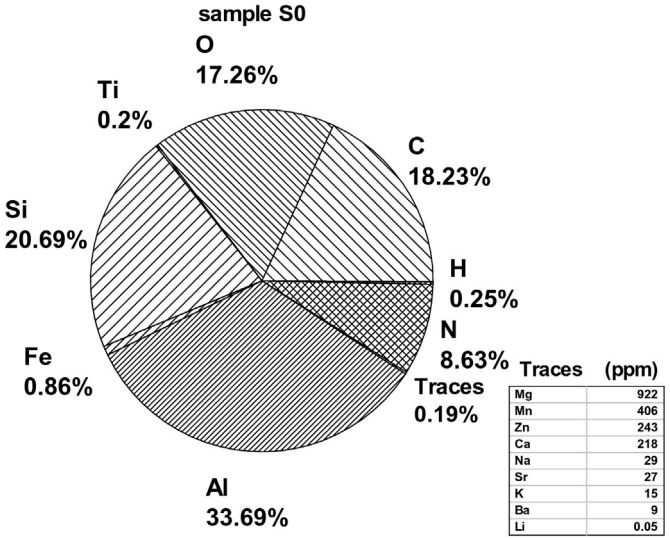

Fig. 6. Major (wt%), minor (wt%), and relevant trace (ppm) element compositions for virgin sand sample (S0).

Table 2
Metal concentrations for waste foundry sands examined.
Note that they are expressed in wt% for major and minor components, and in ppm for trace elements.

Samples	Metal concentrations by LIBS										
	Al wt%	Fe wt%	Ba ppm	Li ppm	Mg ppm	Mn ppm	Ti ppm	Pb ppm	Zr ppm	Zn ppm	Total wt%
S0	33.7	0.9	9.1	0.05	921.6	405.7	2018.0	–	243.4	–	34.9
S1	51.7	0.8	12.5	0.09	607.5	357.9	751.0	–	162.9	–	52.7
S2	34.1	0.8	12.5	0.03	1057.9	431.7	483.7	–	88.2	–	35.1
S3	43.4	1.0	16.5	0.09	840.6	420.9	1100.8	–	345.0	–	44.7
S4	44.1	0.8	11.1	0.06	853.9	289.4	736.5	368.9	162.6	–	45.2
S5	45.2	0.7	12.4	0.08	966.5	719.2	613.3	–	457.0	341.3	46.2
S6	55.0	0.9	17.2	0.14	851.1	574.5	866.2	–	4397.4	463.8	56.6
S7	37.6	2.0	39.5	0.16	2841.1	2002.8	1924.1	–	952.7	–	40.4

The compositional analysis was focused in metal concentrations in WFS in order to assess their potential beneficial use. The concentrations of Al, Ba, Fe, Li, Mg, Mn, Pb, Ti, Zr, and Zn were determined in the different samples (Table 2). The metal compositional ranges obtained for WFS (i.e., samples S1–S7) are summarized in Fig. 7. By comparing these values to those obtained from sample S0, it was found that the total trace metal concentrations in the WFS were greater than those found in sample S0, with the exception of sample S2. This suggests that metals were derived from the metal cast and/or the chemical binders (e.g., clays, coal, and resins) added to the molds and cores (Fig. 8).

The analysis of heavy metal traces is of paramount relevance since they can be harmful to human and animal health if found at elevated concentrations in the environment. In four of the WFS analyzed, concentrations of Ba, Zr, Zn, and Pb were found considerably elevated respect to their natural concentrations in sample S0 (Fig. 9). The Ba concentration (39 ppm) was elevated in sample S7 respect to sample S0 (9 ppm). Ba result commonly elevated as a result of additives added to green sands in ductile iron foundry. The elevated Zr concentration (4397 ppm) found in sample S6 respect to sample S0 (243 ppm) may be attributed to the fact that it is the main constituent of paints used in the molds. In turn, Pb and Zn, that were not detected in sample S0 above their respective LIBS detection limits, were present at significant concentrations in samples S4 (370 ppm Pb), S5 (340 ppm Zn), and S6 (460 ppm Zn). The concentrations of Zn may be due to the presence of this metal in the poured metals, i.e., bronze. The Pb concentration can be due to either bronze casting or the use of this metal in alkyd urethane resin.

5. Conclusions

LIBS technique was successfully applied for the analysis of elemental composition of waste foundry sands. Spectral lines characteristic of several metals; i.e.: Al, Ba, Fe, Li, Mg, Mn, Pb, Ti, Zr, and Zn, were measured and their concentrations quantitatively determined via the calibration-free approach, that is, without the use of calibration standards. The laser-induced plasma was accurately characterized through the calculus of the temperature and the electron density.

The elemental analysis showed that the total metal concentrations in waste sands were increased respect to virgin sand. In particular, the results provided valuable evidence on the relatively elevated concentration of heavy metals, i.e., Ba, Zn, Zr, and Pb, found in four of the samples analyzed as a consequence of the casting material as well as chemical binders used for sand reclaiming.

Overall, our results demonstrated the feasibility of LIBS technique for the rapid screening of metal concentrations in geological samples with complex matrices such as waste sands generated from industrial manufacturing activities. It should be mentioned that LIBS is not competitive but complementary to other analytical techniques. In fact, it allows a pre-selection of samples and analytes of interest which, if necessary, would be later examined with a more accurate laboratory technique.

Acknowledgments

This work was supported by the Concejo Nacional de Investigaciones Científicas y Técnicas (CONICET) through a PostDoctoral research grant.

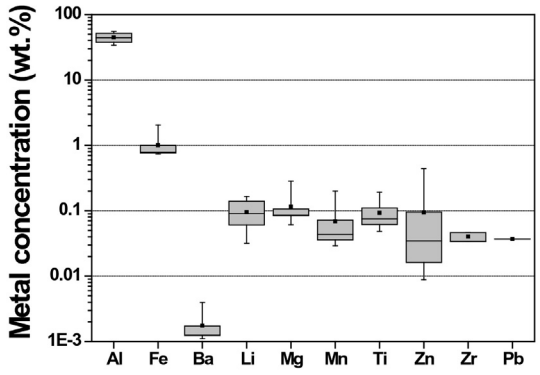

Fig. 7. Composition range for metals determined in waste foundry sands. Box plot: whisker range: min–max; Box: 25th percentile, median, 75th percentile; Mean (■).

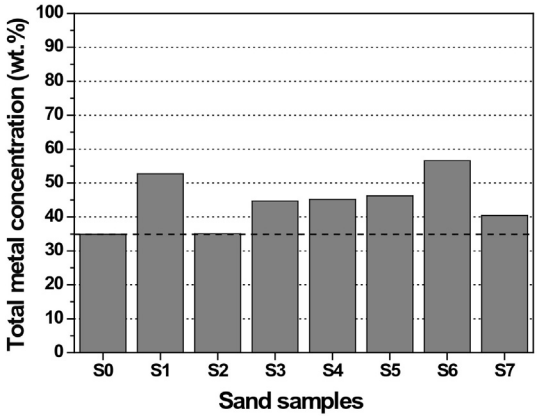

Fig. 8. Comparison of total metal concentrations between waste foundry sands samples (S1–S7) and virgin sand sample (S0).

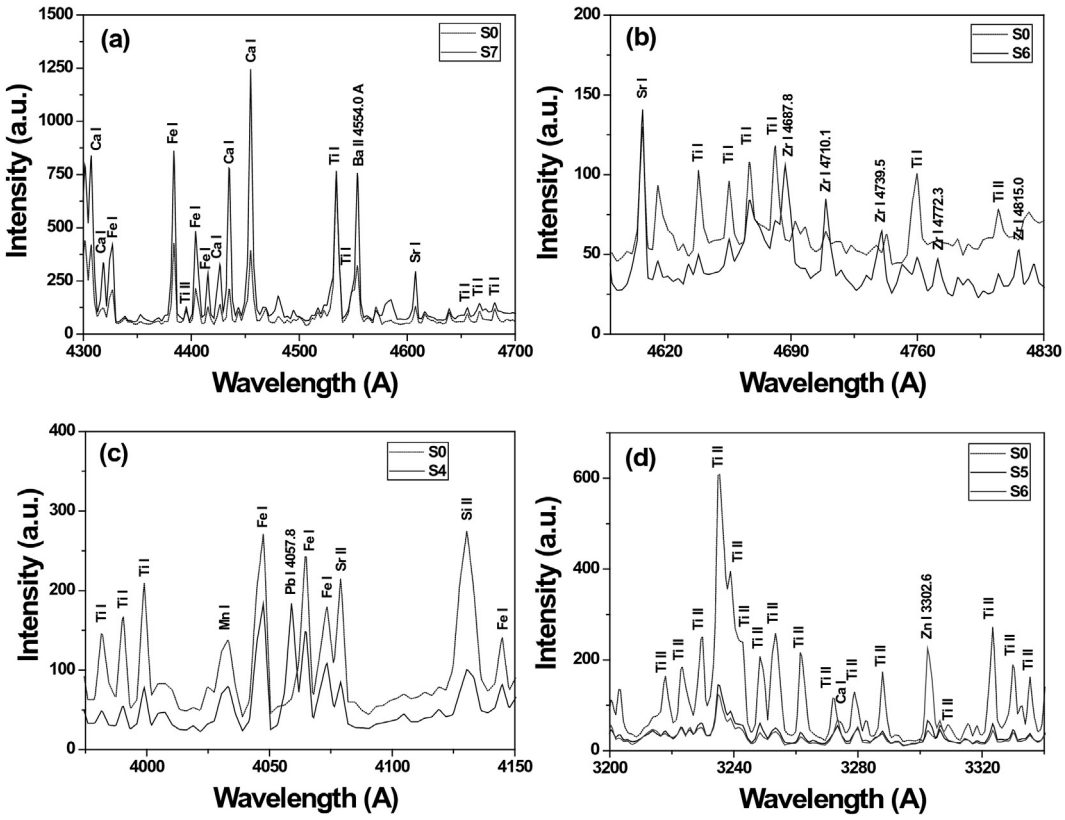

Fig. 9. Comparison of LIBS spectra for virgin sand (S0) and heavy metal-contaminated waste foundry sands (S4, S5, S6, S7).

References

[1] R.L.P. Carnin, M. Valadares Folgueras, R.R. Luvizão, S.L. Correia, C.J. da Cunha, R.S. Dungan, Use of an integrated approach to characterize the physicochemical properties of foundry green sands, Thermochim. Acta 543 (2012) 150–155.

[2] R.E. Miguel, J.A. Ippolito, A.A. Porta, R.B. Banda Noriega, R.S. Dungan, Use of standardized procedures to evaluate metal leaching from waste froundry sands, J. Environ. Qual. 42 (2013) 1–6.

[3] B.J. Lindsay, T.J. Logan, Agricultural reuse of foundry sand, J. Residuals Sci. Tech. 2 (2005) 3–12.

[4] R. Siddique, G. Schutter, A. Noumowe, Effect of used-foundry sand on the mechanical properties of concrete, Constr. Build. Mater. 23 (2009) 976–980.

[5] R.E. Miguel, J.A. Ippolito, A.B. Leytem, A.A. Porta, R.B. Banda Noriega, R.S. Dungan, Analysis of total metals in waste molding and core sands from ferrous and non-ferrous foundries, J. Environ. Manag. 110 (2012) 77–81.

[6] J.D. Winefordner, I.B. Gornushkin, T. Correll, E. Gibb, B.W. Smith, N. Omenetto, Comparing several atomic spectrometric methods to the super stars: special emphasis on laser induced breakdown spectrometry, LIBS, a future super star, J. Anal. At. Spectrom. 19 (2004) 1061–1083.

[7] R.S. Harmon, R.E. Russo, R.R. Hark, Applications of laser-induced breakdown spectroscopy for geochemical and environmental analysis: a comprehensive review, Spectrochim. Acta B 87 (2013) 11–26.

[8] A.W. Miziolek, V. Palleschi, I. Schechter, Laser Induced Breakdown Spectroscopy, Cambridge University Press, Cambridge, 2006.

[9] D.A. Cremers, L.J. Radziemski, Handbook of Laser-induced Breakdown Spectroscopy, Wiley, Chichester, 2006.

[10] J.P. Singh, S.N. Thakur, Laser-Induced Breakdown Spectroscopy, Elsevier, Amsterdam, 2007.

[11] C. Pasquini, J. Cortez, L.M.C. Silva, F.B. Gonzaga, Laser induced breakdown spectroscopy, J. Braz. Chem. Soc. 18 (2007) 463–512.

[12] E. Tognoni, V. Palleschi, M. Corsi, G. Cristoforetti, N. Omenetto, I. Gorhushkin, B.W. Smith, J.D. Winefordner, From sample to signal in laser-induced breakdown spectroscopy: a complex route to quantitative analysis, in: A.W. Miziolek, V. Palleschi, I. Schechter (Eds.), Laser-induced Breakdown Spectroscopy (LIBS) Fundamentals and Applications, Cambridge University Press, New York 2006, pp. 122–170.

[13] D.W. Hahn, N. Omenetto, Laser-induced breakdown spectroscopy (LIBS), part I: review of basic diagnostics and plasma–particle interactions: still-challenging issues within the analytical plasma community, Appl. Spectrosc. 64 (2010) 335A–366A.

[14] D.W. Hahn, N. Omenetto, Laser-Induced Breakdown Spectroscopy (LIBS), part II: review of instrumental and methodological approaches to material analysis and applications to different fields, Appl. Spectrosc. 66 (2012) 347–419.

[15] E. Tognoni, G. Cristoforetti, S. Legnaioli, V. Palleschi, Calibration-free laser-induced breakdown spectroscopy: state of the art, Spectrochim. Acta B 65 (2010) 1–14.

[16] R.S. Harmon, R.E. Russo, R.R. Hark, Applications of laser-induced breakdown spectroscopy for geochemical and environmental analysis: a comprehensive review, Spectrochim. Acta B 87 (2013) 11–26.

[17] G.S. Senesi, Laser-Induced Breakdown Spectroscopy (LIBS) applied to terrestrial and extraterrestrial analogue geomaterials with emphasis to minerals and rocks, Earth Sci. Rev. 139 (2014) 231–267.

[18] R. Krasniker, V. Bulatov, I. Schechter, Study of matrix effects in laser plasma spectroscopy by shock wave propagation, Spectrochim. Acta B 56 (2001) 609–618.

[19] R.D. Harris, D.A. Cremers, M.H. Ebinger, B.K. Bluhm, Determinations of nitrogen in sand using laser-induced breakdown spectroscopy, Appl. Spectrosc. 58 (2004) 770–775.

[20] A.F.M.Y. Haider, M. Wahadoszamen, M.E. Sadat, K.M. Abedin, A.I. Talukder, Elemental profiling and determination of Ti content of the beach sand samples of Bangladesh using LIBS technique, Opt. Laser Technol. 42 (2010) 969–974.

[21] K.M. Abedin, A.F.M.Y. Haider, M.A. Rony, Z.H. Khan, Identification of multiple rare earths and associated elements in raw monazite sands by laser-induced breakdown spectroscopy, Opt. Laser Technol. 43 (2011) 45–49.

[22] E. Tognoni, G. Cristoforetti, S. Legnaioli, V. Palleschi, A. Salvetti, M. Muelle, U. Panne, I. Gornushkin, A numerical study of expected accuracy and precision in Calibration-Free Laser-Induced Breakdown Spectroscopy in the assumption of ideal analytical plasma, Spectrochim. Acta B 62 (2007) 1287–1302.

[23] H.R. Griem, Principles of Plasma Spectroscopy, Cambridge University Press, Cambridge, 1997.

[24] Evaluation of plasma parameters in optically thick plasmas, in: H. Zwicker, W. Lochte-Holtgreven (Eds.), Plasma Diagnostics, North-Holland Publishing Company, Amsterdam 1968, pp. 214–248.

[25] C. Aragón, J.A. Aguilera, Characterization of laser induced plasmas by optical emission spectroscopy: a review of experiments and methods, Spectrochim. Acta B 63 (2008) 893–916.

[26] A.M. El Sherbini, H. Hegazy, T.M. El Sherbini, Measurement of electron density utilizing the H Alpha-line from laser produced plasma in air, Spectrochim. Acta B 61 (2006) 532–539.

[27] H.R. Griem, Spectral Line Broadening by Plasmas, Academic Press, New York, 1974.

[28] A. Bertolini, G. Carelli, F. Francesconi, M. Francesconi, L. Marchesini, P. Marsili, F. Sorrentino, G. Cristoforetti, S. Legnaioli, V. Palleschi, L. Pardini, A. Salvetti, Modì: a new mobile instrument for in situ double-pulse LIBS analysis, Anal. Bioanal. Chem. 385 (2006) 240–247.

[29] Marwan Technology, http://www.marwan-technology.com/.

[30] S. Pagnotta, E. Grifoni, S. Legnaioli, M. Lezzerini, G. Lorenzetti, V. Palleschi, Comparison of brass alloys composition by laser-induced breakdown spectroscopy and self-organizing maps, Spectrochim. Acta B 103–104 (2015) 70–75.
[31] G. Agrosì, G. Tempesta, E. Scandale, S. Legnaioli, G. Lorenzetti, S. Pagnotta, V. Palleschi, A. Mangone, M. Lezzerini, Application of Laser Induced Breakdown Spectroscopy to the identification of emeralds from different synthetic processes, Spectrochim. Acta B 102 (2014) 48–51.
[32] M. Tofanelli, L. Pardini, M. Borrini, F. Bartoli, A. Bacci, A. D'Ulivo, E. Pitzalis, M.C. Mascherpa, S. Legnaioli, G. Lorenzetti, S. Pagnotta, G. De Holanda Cavalcanti, M. Lezzerini, V. Palleschi, Spectroscopic analysis of bones for forensic studies, Spectrochim. Acta B 99 (2014) 70–75.
[33] S. Legnaioli, G. Lorenzetti, L. Pardini, G.H. Cavalcanti, V. Palleschi, Applications of LIBS to the analysis of metals, Springer Series in Opt. Sci. 82 (2014) 169–193.
[34] G.H. Cavalcanti, A.A. Rocha, R.N. Damasceno, S. Legnaioli, G. Lorenzetti, L. Pardini, V. Palleschi, Double-pulse laser-induced breakdown spectroscopy analysis of scales from petroleum pipelines, Spectrochim. Acta B 87 (2013) 188–191.
[35] E. Grifoni, S. Legnaioli, M. Lezzerini, G. Lorenzetti, S. Pagnotta, V. Palleschi, Extracting time-resolved information from time-integrated laser-induced breakdown spectra, J. Spectrosc. 1–5 (2014).
[36] NIST Electronic Database, http://physics.nist.gov/PhysRefData.
[37] D. Bulajic, M. Corsi, G. Cristoforetti, S. Legnaioli, V. Palleschi, A. Salvetti, E. Tognoni, A procedure for correcting self-absorption in calibration free laser induced breakdown spectroscopy, Spectrochim. Acta B 57 (2002) 339–353.
[38] A.M. El Sherbini, Th.M.El Sherbini, H. Hegazy, G. Cristoforetti, S. Legnaioli, V. Palleschi, L. Pardini, A. Salvetti, E. Tognoni, Evaluation of self-absorption coefficients of aluminum emission lines in laser-induced breakdown spectroscopy measurements, Spectrochim. Acta B 60 (2005) 1573–1579.
[39] F. Brédice, F.O. Borges, H. Sobral, M. Villagrán-Muñiz, H.O. Di Rocco, G. Cristoforetti, S. Legnaioli, V. Palleschi, L. Pardini, A. Salvetti, E. Tognoni, Evaluation of self-absorption of manganese emission lines in Laser Induced Breakdown Spectroscopy measurements, Spectrochim. Acta B 61 (2006) 1294–1303.
[40] J.A. Aguilera, C. Aragón, Characterization of laser-induced plasmas by emission spectroscopy with curve-of-growth measurements. Part I: temporal evolution of plasma parameters and self-absorption, Spectrochim. Acta B 63 (2008) 784–792.
[41] H.Y. Moon, K.K. Herrera, N. Omenetto, B.W. Smith, J.D. Winefordner, On the usefulness of a duplicating mirror to evaluate self-absorption effects in laser induced breakdown spectroscopy, Spectrochim. Acta B 64 (2009) 702–713.
[42] F. Brédice, H.O. Di Rocco, H.M. Sobral, M. Villagrán-Muñiz, V. Palleschi, A new method for determination of self-absorption coefficients of emission lines in Laser-induced breakdown spectroscopy experiments, Appl. Spectrosc. 64 (2010) 320–323.
[43] D.M. Díaz Pace, C.A. D'Angelo, G. Bertuccelli, Study of self-absorption of emission magnesium lines in laser-induced plasmas on calcium hydroxide matrix, IEEE Trans. Plasma Sci. 40 (2012) 898–908.
[44] I.B. Gornushkin, C.L. Stevenson, B.W. Smith, N. Omenetto, J.D. Winefordner, Modeling an inhomogeneous optically thick laser induced plasma: a simplified theoretical approach, Spectrochim. Acta B 56 (2001) 1769–1785.
[45] T. Sakka, T. Nakajima, Y.H. Ogata, Spatial population distribution of laser ablation species determined by self-reversed emission line profile, J. Appl. Phys. 92 (2002) 2296–2303.
[46] I.B. Gornushkin, N. Omenetto, B.W. Smith, J.D. Winefordner, Determination of the maximum temperature at the center of an optically thick laser-induced plasma using self-reversed spectral lines, Spectrochim. Acta B 59 (2004) 401–418.
[47] A.Y. Kazakov, I.B. Gornushkin, N. Omenetto, B.W. Smith, J.D. Winefordner, Radiation dynamics of post-breakdown laser induced plasma expanding into ambient gas, Appl. Opt. 45 (2006) 2810–2820.
[48] C.A. D'Angelo, D.M. Díaz Pace, G. Bertuccelli, D. Bertuccelli, Laser induced breakdown spectroscopy on metallic alloys: solving inhomogeneous optically thick plasmas, Spectrochim. Acta Part B 63 (2008) 367–374.
[49] C.A. D'Angelo, D.M. Díaz Pace, G. Bertuccelli, Semiempirical model for analysis of inhomogeneous optically thick laser-induced plasmas, Spectrochim. Acta B 64 (2009) 999–1008.
[50] D.M. Díaz Pace, Laser-induced plasma characterization using line profile analysis of chromium neutral atom and ion transitions, J. Quant. Spectrosc. Radiat. Transf. 129 (2013) 254–262.
[51] C.G. Parigger, D.M. Surmick, G. Gautam, A.M. El Sherbini, Hydrogen alpha laser ablation plasma diagnostics, Op. Lett. 40 (2015) 3436–3439.
[52] H.O. Di Rocco, F. Brédice, V. Palleschi, The calculation of the optical depths of homogeneous plasmas: analytical, experimental, and numerical considerations, Appl. Spectrosc. 65 (10) (2011) 1–5.
[53] R.W.P. McWhirter, in: R.H. Huddlestone, S.L. Leonard (Eds.), Plasma Diagnostic Techniques, Academic Press, New York 1965, pp. 201–264 (Chapter 5).
[54] J.A. Aguilera, C. Aragón, Characterization of a laser-induced plasma by spatially resolved spectroscopy of neutral atom and ion emissions. Comparison of local and spatially integrated measurements, Spectrochim. Acta B 59 (2004) 1861–1876.